SUPPORTING INFORMATION

Fe(III)-carboxythiolate layered Metal-Organic Frameworks with potential interest as active materials for rechargeable alkali-ion batteries

*Nusik Gedikoglu,[a‡] Pablo Salcedo-Abraira,[a‡] Long H.B. Nguyen,[b,d] Nathalie Guillou,[c] Nicolas Dupré,[a] Christophe Payen,[a] Nicolas Louvain,[b,d] Lorenzo Stievano,[b,d] Philippe Poizot,[a] and Thomas Devic[a]**

a. Nantes Université, CNRS, Institut des Matériaux de Nantes Jean Rouxel, IMN, F-44000 Nantes, France.

b. ICGM, Univ. Montpellier, CNRS, ENSCM, Montpellier, France

c. Institut Lavoisier de Versailles, UMR CNRS 8180, Université de Versailles St-Quentin en Yvelines, Université Paris Saclay, 78035 Versailles, France.

d. Réseau sur le Stockage Electrochimique de l'Energie (RS2E), FR CNRS 3459, Amiens, France

1. Synthesis of H_4DSBDC

2,5-disulfhydrylbenzene-1,4-dicarboxylic acid (H_4DSBDC) was synthesized based on the procedure published by Vial et al.[1]

^{1}H NMR (300MHz, DMSO-d6): δ (ppm) = 8.03 (s, 2H, Ar-H); 13C NMR (500MHz, DMSO-d6): δ (ppm) = 166.67, 133.16, 133.14, 130.00.

FTIR (Diamond-ATR, cm^{-1}): 2958 (m, b), 2863 (m, b), 2815 (m, b), 2646 (m), 2545 (m), 2506 (m), 1685 (vs), 1474 (m), 1409 (s), 1349 (w), 1295 (m), 1251 (s), 1148 (w), 1094 (w), 974 (w), 925 (w), 904 (m), 782 (m), 635 (m), 554 (w), 510 (w), 435 (w);

MS (ESI, m/z): 229 (M-H-, 100%).

Elemental analysis calculated for $C_8H_6O_4S_2$: C, 41.72; H, 2.63; S, 27.85. Found: C, 41.77; H, 2.59; S, 27.69.

2. Chemical analysis of the MOFs

The purity of each phase was assessed by a combination of elemental analysis (C, H, S) and ICP-AES (Fe, Na, K). Values are given in wt%, with their standard deviation based on multiple analyses

(DMA){Fe(DSBDC)}: theo. C 36.59, H 3.07, N 4.26, S 19.54, O 19.50, Fe 17.01; exp. C 36.4 ± 0.1, H 3.06 ± 0.01, N 4.59 ± 0.03, S 14.6 ± 2.2, Fe 17.0 ± 0.2;

Na{Fe(DSBDC)}·2.5H_2O theo. C 27.44, H 2.01, S 18.31, O 29.70, Fe 15.95, Na 6.56; exp. C 27.19 ± 0.04, H 1.83 ± 0.01, S 16.7 ± 0.8, Fe 16.5 ± 0.2, Na 6.17 ± 0.1;

K{Fe(DSBDC)}·nH_2O theo. C 26.23, H 1.92, S 17.51, O 28.39, Fe 15.24, K 10.67; exp. C 25.63 ± 0.06, H 1.63 ± 0.01, S 16.3 ± 2.8, Fe 15.9 ± 0.2, K 11.9 ± 0.5.

3. Structural characterization

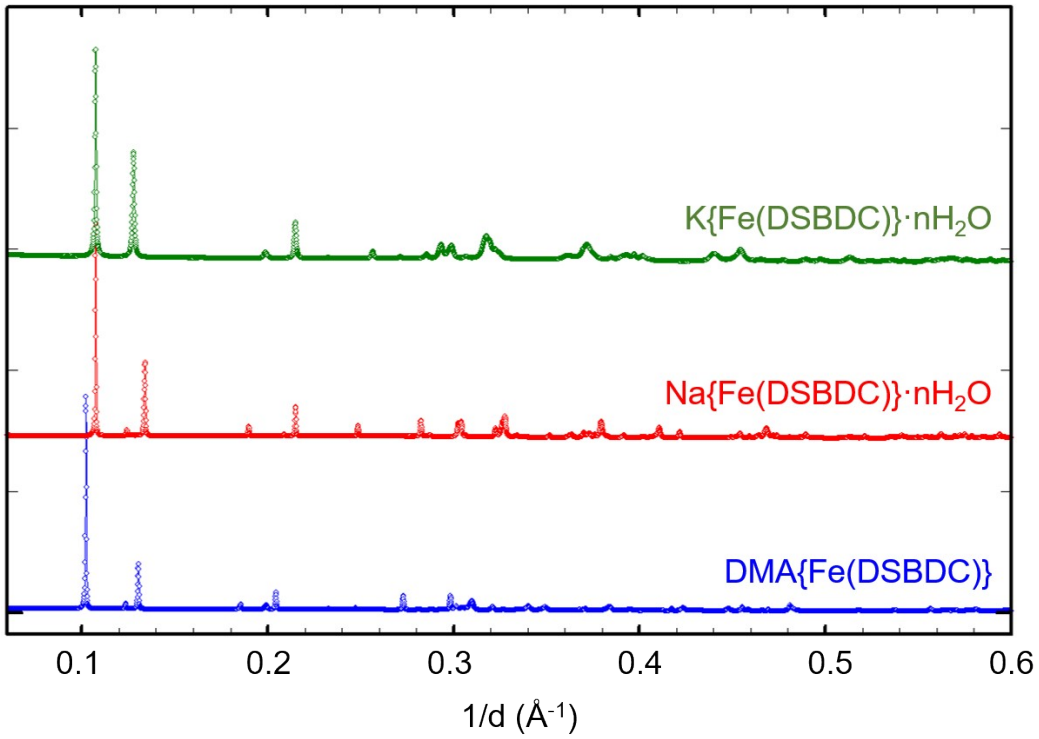

Figure S1. PXRD patterns of (DMA){Fe(DSBDC)}, Na{Fe(DSBDC)}·2.5H_2O and K{Fe(DSBDC)}·nH_2O.

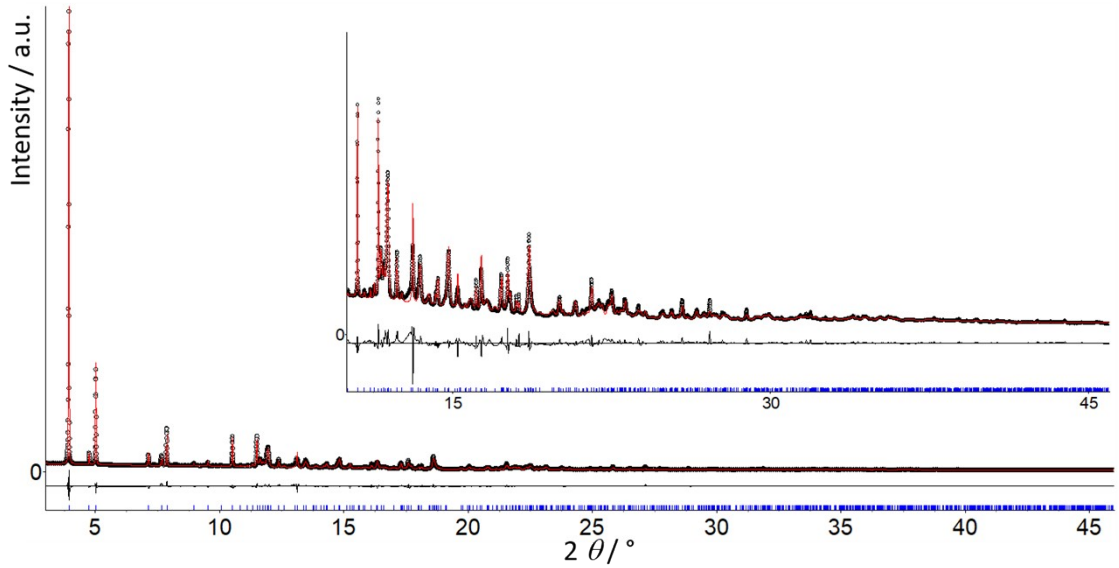

Figure S2. Rietveld plot of (DMA){Fe(DSBDC)} using the SCXRD structural model, with only refinement of the profile parameters. R_{wp} = 0.064 and R_{Bragg} = 0.026 ($\lambda_{synchrotron}$ = 0.671415Å).

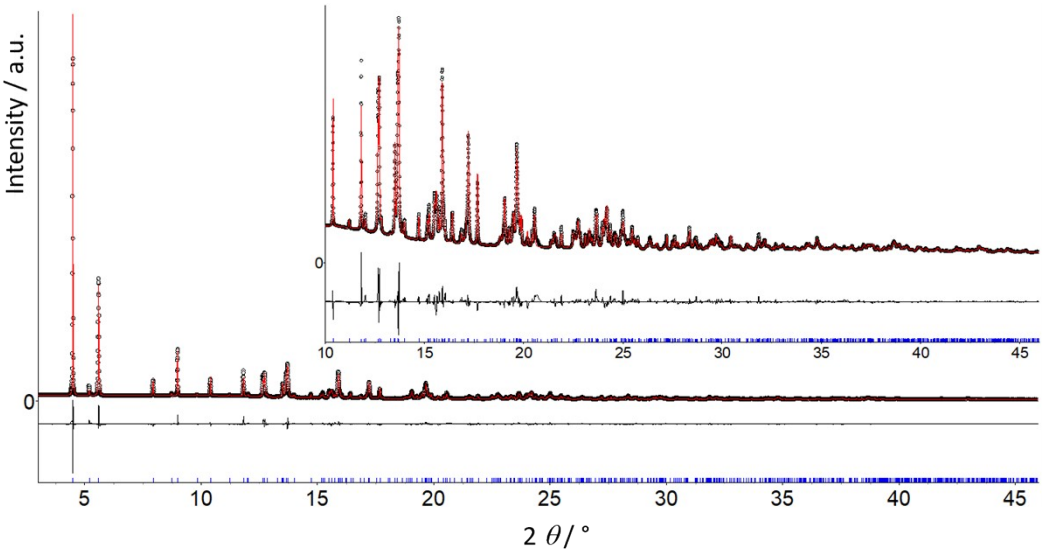

Figure S3. Final Rietveld plot of Na{Fe(DSBDC)}·2.5H_2O. R_{wp} = 0.051 and R_{Bragg} = 0.038 ($\lambda_{synchrotron}$ = 0.72890 Å).

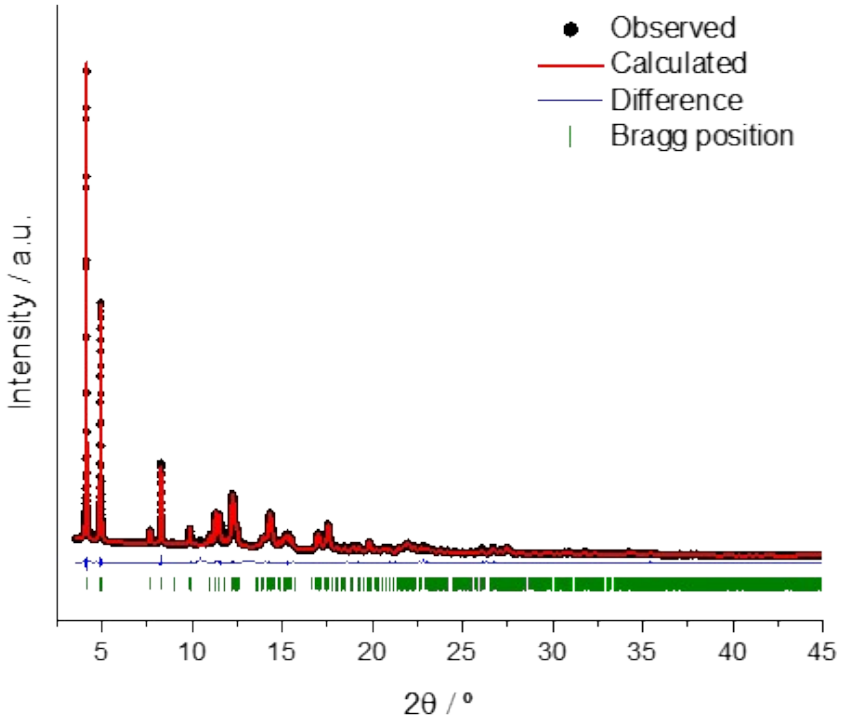

Figure S4. Whole structureless powder pattern fitting of K{Fe(DSBDC)}·nH_2O. R_{wp} = 0.030 ($\lambda_{synchrotron}$ = 0.671415 Å).

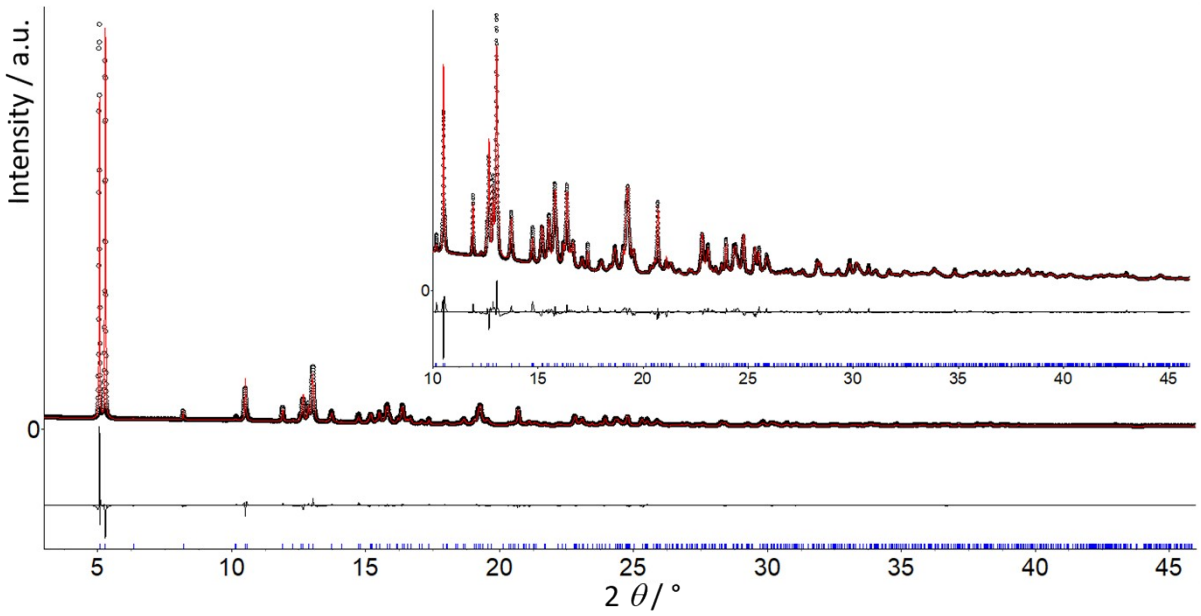

Figure S5. Final Rietveld plot of Na{Fe(DSBDC)}. R_{wp} = 0.036 and R_{Bragg} = 0.040 ($\lambda_{synchrotron}$ = 0.72890 Å).

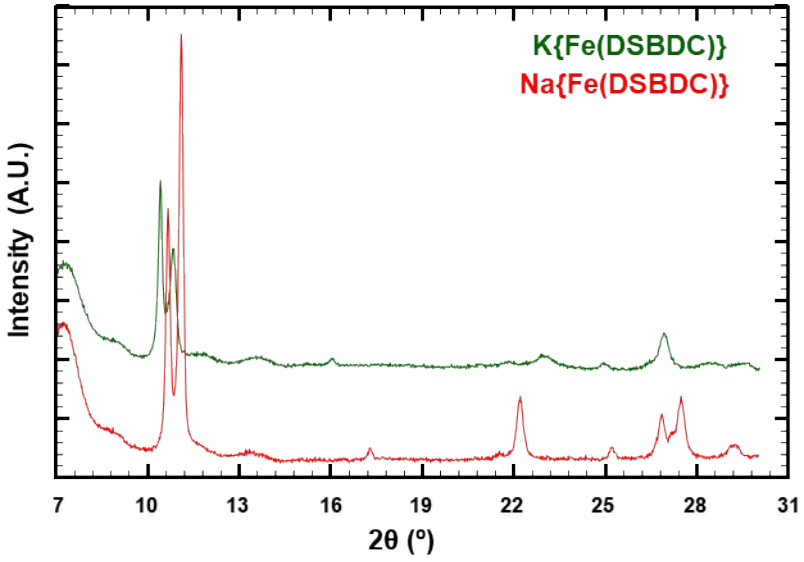

Figure S6. Comparison of the PXRD patterns of Na{Fe(DSBDC)} and K{Fe(DSBDC)} ($\lambda_{CuK\alpha}$ = 1.5418 Å).

Table S1. Crystallographic information of (DMA){Fe(DSBDC)}.

Formula	$C_{10}H_{10}FeNO_4S_2$
Formula weight / g	328.16
Temperature / K	297(2)
Wavelength / Å	Mo Kα, 0.71073
Crystal dimensions / mm^3	0.03 x 0.005 x 0.005
Crystal system	Triclinic
Space group	*P*-1
a / Å	3.5583(4)
b / Å	8.598(2)
c / Å	10.405 (2)
α / °	109.90 (2)
β / °	92.47 (1)
γ / °	91.71 (1)
V / $Å^3$	298.71(8)
Z (molecules / cell)	1
D_{calc} / *g* cm^{-3}	1.824
Absorption coefficient / mm^{-1}	1.615
F(000)	167
Theta range for data collection	3.784 to 26.331
Index ranges	$-4 \leq h \leq 4$
	$-10 \leq k \leq 10$
	$-12 \leq l \leq 12$
Reflections collected	8852
Independent reflections	1227
Completeness to theta = 25.24°	99.7%
Max. and min. transmission	1.0000, 0.2926
Data / restraints / parameters	1227/3/82
Goodness-of-fit on F^2	1.215
Final R indices [I>2sigma(I)]	R_1, wR_2= 0.1231, 0.2505
R indices (all data)	R_1, wR_2= 0.1578, 0.2644
Largest diff. peak and hole	0.908, -0.773

Table S2. Crystallographic information of Na{Fe(DSBDC)}·2.5H_2O and Na{Fe(DSBDC)}.

Compound	Na{Fe(DSBDC)}·2.5H_2O	Na{Fe(DSBDC)}
Crystal system	Triclinic	Triclinic
Wavelength / Å	0.72890	0.72890
Space group	*P*-1	*P*-1
a / Å	3.5487(1)	3.55430(4)
b / Å	8.5445(2)	8.5345(1)
c / Å	10.0485(2)	10.2606 (1)
α / °	109.249(2)	128.8186(7)
β / °	100.613(2)	95.899(1)
γ / °	90.723(2)	91.179(2)
V / Å^3	281.85(2)	239.763(6)
R_{wp}	0.051	0.036
R_{Bragg}	0.038	0.040

Table S3. Na-O bond distances and O-Na-O bond angles in Na{Fe(DSBDC)}·2.5H_2O and Na{Fe(DSBDC)}.

Compound	Na{Fe(DSBDC)}·2.5H_2O	Na{Fe(DSBDC)}
	Bond length / Å	
Na1-O2 (-COO)	2.364(5)	2.451(4)
Na1-O2B (-COO)	2.390(4)	2.364(4)
Na1-O1 (-COO)		2.523(4)
Na1-Ow1 (H_2O)	2.467(5)	
	Bond angle / °	
O2-Na1-O2C (chain)	83.4(2)	84.9(2)
O1-Na1-O2 (chelating carboxylate)		53.6(1)

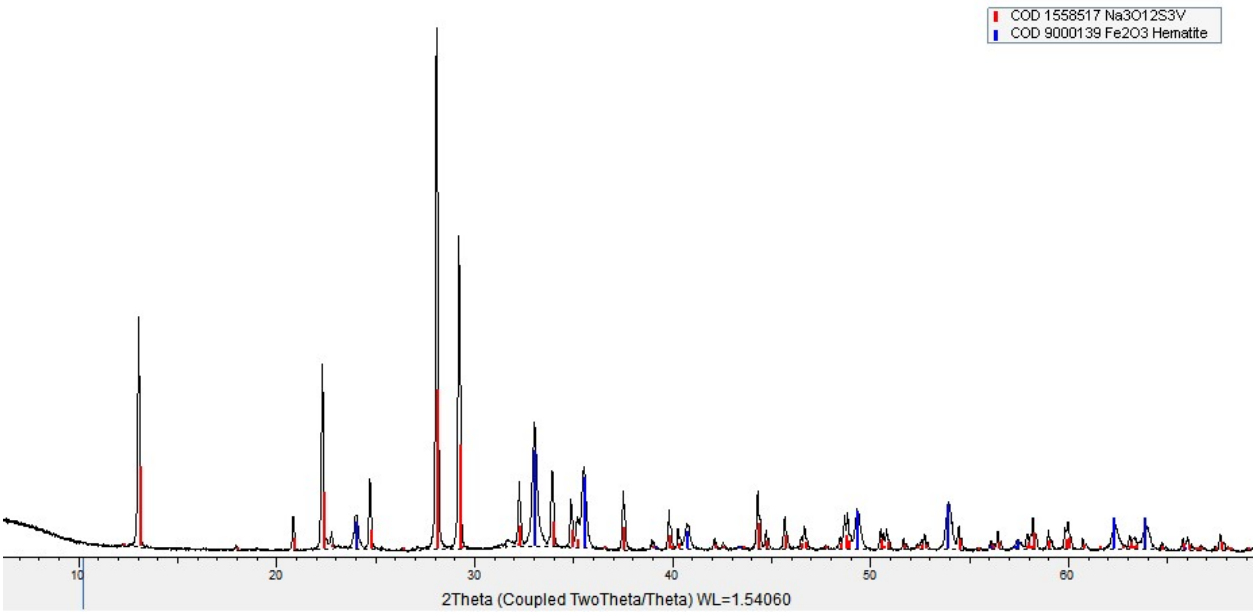

Figure S7. PXRD pattern of the combustion product of Na{Fe(DSBDC)}·2.5H_2O after calcination at 500°C in air. Mixture is composed of $Na_3Fe(SO_4)_3$ (no CIF available), Fe_2O_3 (COD 9000139), and small amounts of unidentified phase ($\lambda_{Cuk\alpha}$ = 1.5406 Å).

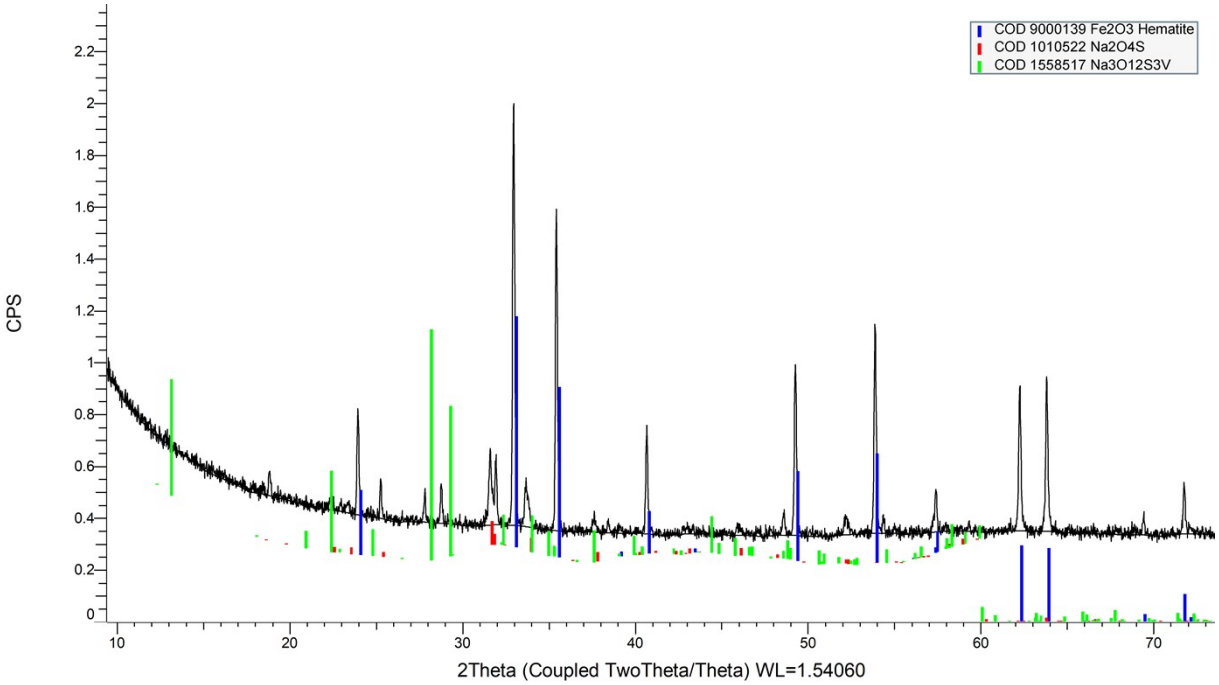

Figure S8. PXRD pattern of the combustion product of Na{Fe(DSBDC)}·2.5H_2O after calcination at 1000°C in air. Mixture is composed of Fe_2O_3 (COD 9000139), Na_2SO_4, $Na_3Fe(SO_4)_3$ and possibly other phases ($\lambda_{CuK\alpha}$ = 1.5406 Å).

4. ^{1}H liquid NMR

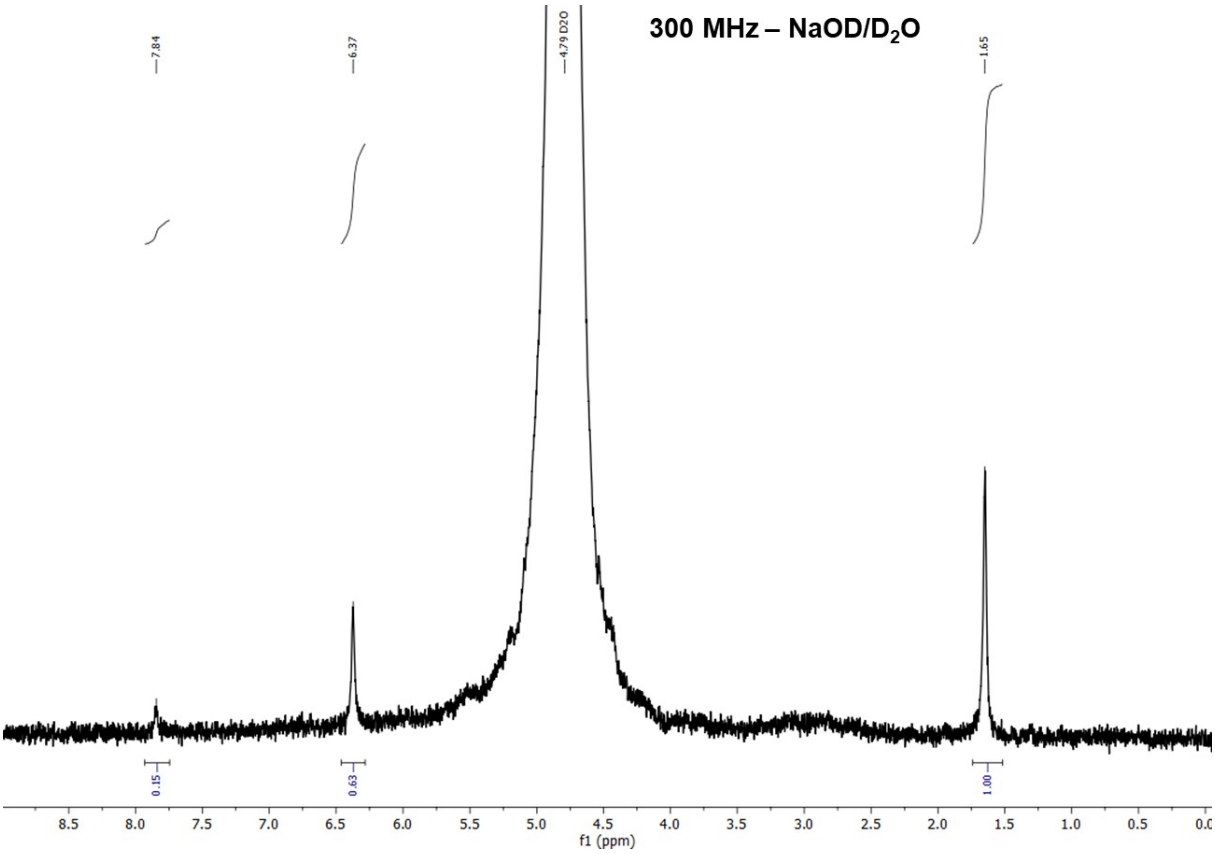

Figure S9. ^{1}H NMR spectrum of the degradation product of DMA{Fe(DSBDC)} in $NaOD/D_2O$. Signals at 7.84, 6.37 and 1.65 are attributed to N-H (DMA), C-H (DSBDC) and CH_3 (DMA).

5. Scanning electron microscopy and electron dispersive spectroscopy

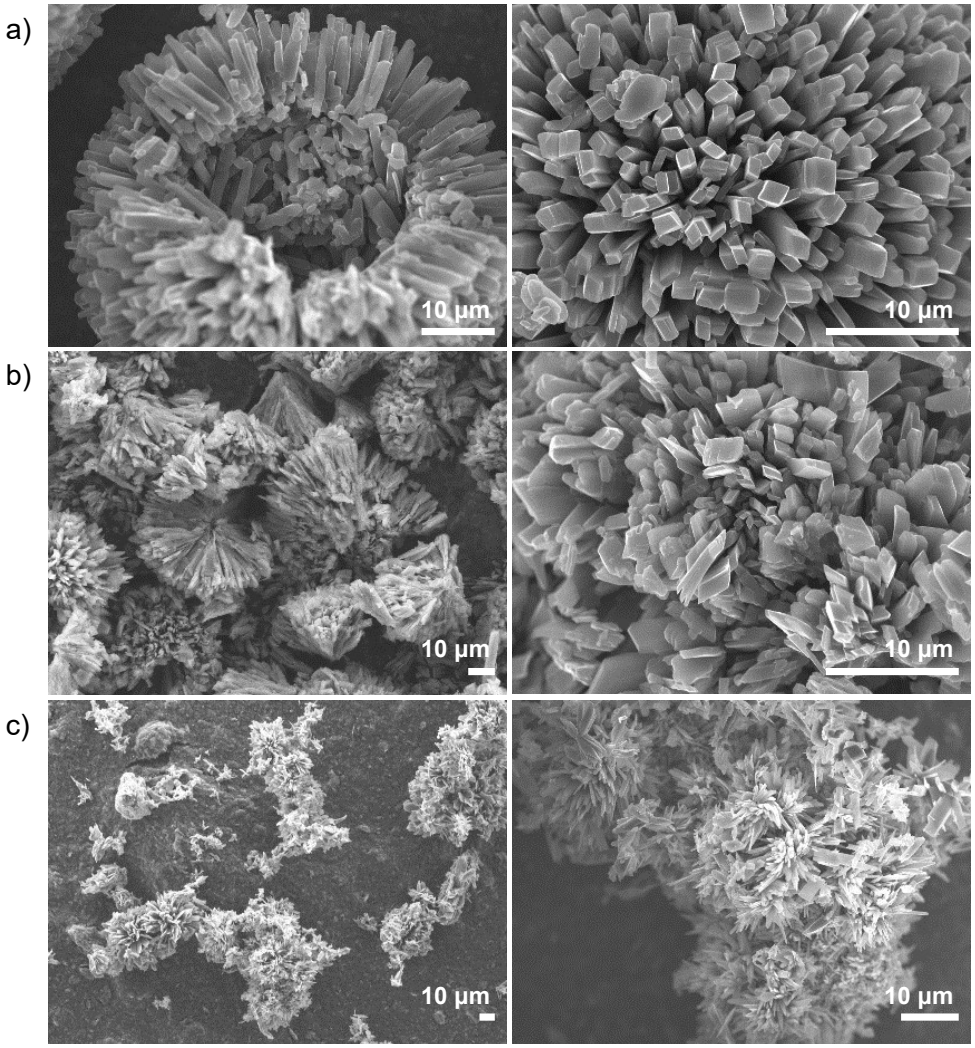

Figure S10. Scanning Electron microscopy images of a) DMA{Fe(DSBDC)}, b) Na{Fe(DSBDC)}·2H_2O and c) K{Fe(DSBDC)}·nH_2O.

Table S4. Average atomic percentage of heavy elements (Fe, S, Na, K) in the three solids.

Compound	Fe (at %)	S (at %)	Na (at %)	K (at %)	Deduced Na,K/Fe/DSBDC
(DMA){Fe(DSBDC)}	3.30	6.88	-	-	-/1.00/1.04
Na{Fe(DSBDC)}·2.5H_2O	4.51	9.00	4.80	-	1.06/1.00/1.00
K{Fe(DSBDC)}·nH_2O	5.43	10.66	-	6.20	1.14/1.00/0.98

6. Infrared spectroscopy

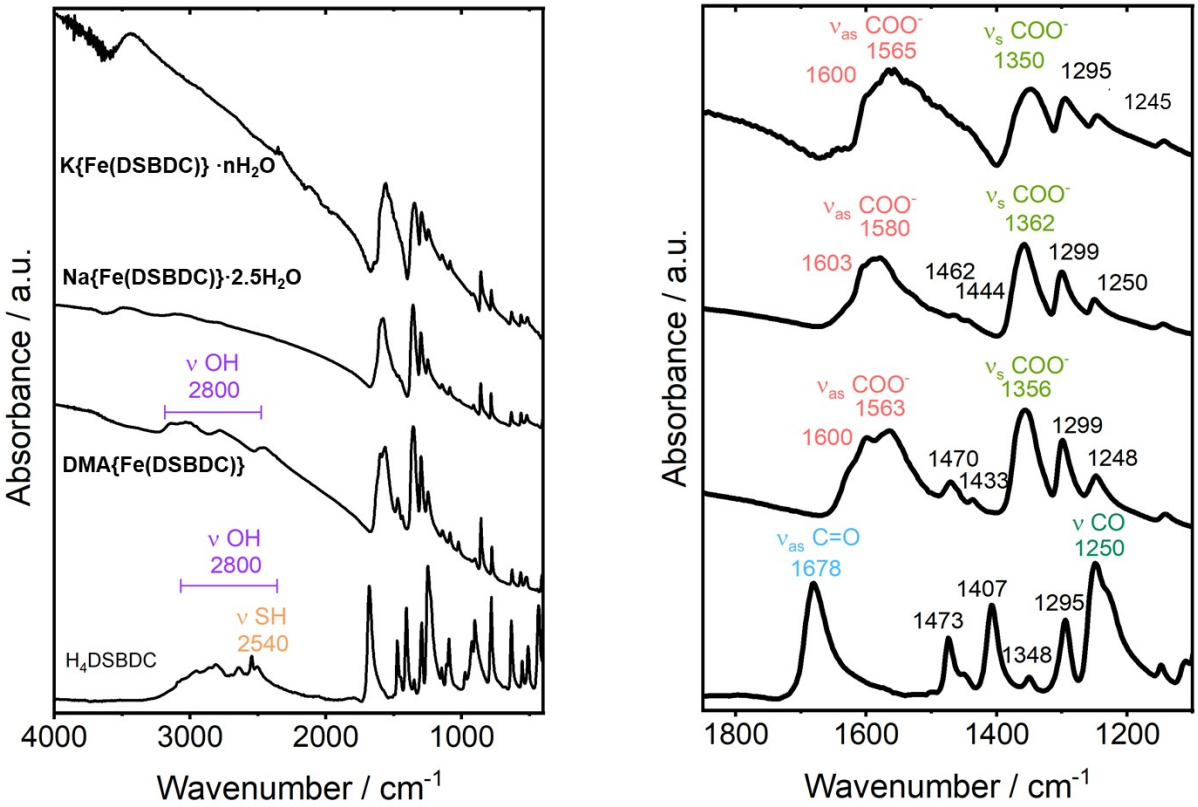

Figure S11. FTIR spectra of H_4DSBDC, (DMA){Fe(DSBDC)}, Na{Fe(DSBDC)}·2.5H_2O and K{Fe(DSBDC)}·nH_2O.

Table S5. IR vibrational bands (in cm^{-1}) and proposed assignments for H_4DSBDC, (DMA){Fe(DSBDC)}, Na{Fe(DSBDC)}·2.5H_2O.

H_4DSBDC		(DMA){Fe(DSBDC)}		Na{Fe(DSBDC)}·2.5H_2O	
2540	ν_s SH				
1678*	ν_{as} C=O	**1544**	ν_{as} COO^-	**1568**	ν_{as} COO^-
1473	ν_s CC, ν_s CO	1468	ν_s CC, ν_s CO	1453	ν_s CC
1407	ν_s CC, ν_s CO	1433	ν_s CC, ν_s CO	1444	ν_s CC
1348	ν_s CC, ν_s CO	**1342**	ν_s COO^-	**1350**	ν_s COO^-
1295	ν_s CC, ν_s CO-H, ν_s CO	1299	ν_s CC, ν_s CO-H, ν_s CO	1299	ν_s CC, ν_s CO
1250	ν_s CO, ν_s CC	1248	ν_s CC	1250	ν_s CC

*most intense peaks are highlighted bold.

7. Thermogravimetric analyses (TGA)

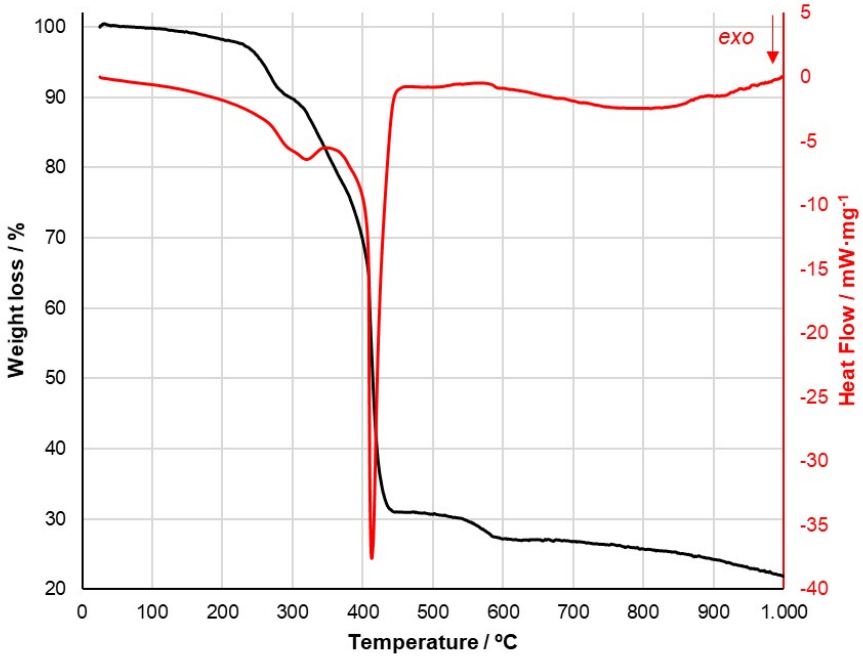

Figure S12. TG-DSC curves of (DMA){Fe(DSBDC)} measured under air at 5°C min^{-1}.

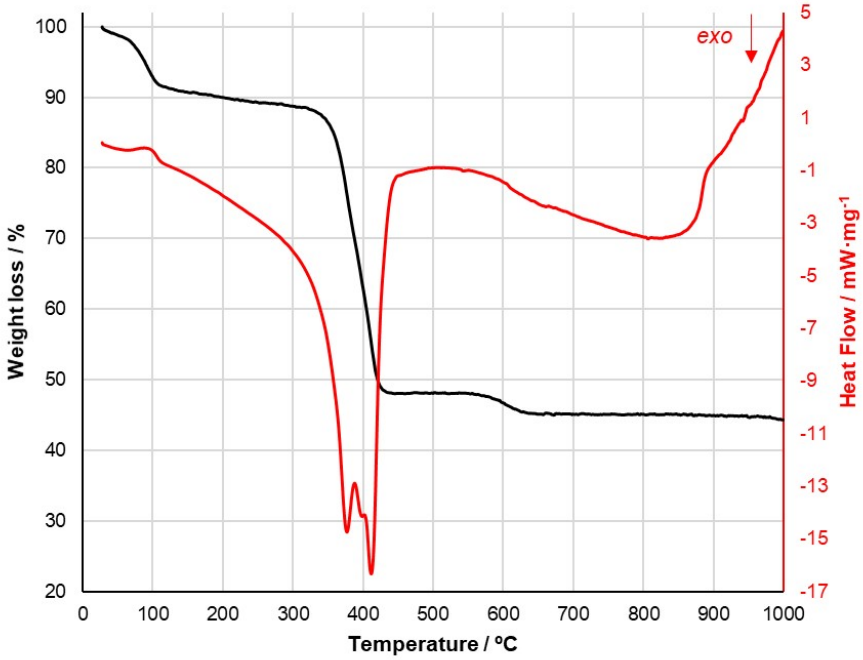

Figure S13. TG-DSC curves of Na{Fe(DSBDC)}·2.5H_2O measured under air at 5°C min^{-1}.

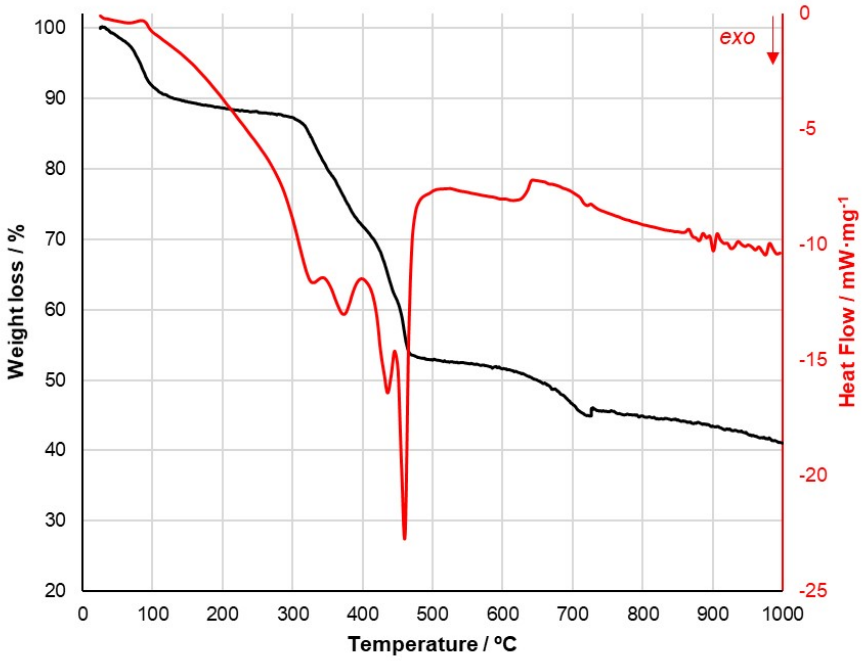

Figure S14. TG-DSC curves of K{Fe(DSBDC)}·nH_2O measured under air at 5°C min^{-1}.

8. Stability tests in DMF, ethanol, and water

The stability of the three solids in DMF, ethanol, and water was evaluated by suspending samples in these solvents and examining signs of degradation at the end of the period by powder X-ray diffraction, infrared spectroscopy and visual inspection of the supernatant. For the tests, 10 mg of solid was suspended in 10 ml of solvent in nearly full closed glass vials. The suspensions were stirred for 1 h, and then left at rest for a determined amount of time. At the end of the period, the compounds were separated from their solvents by centrifugation and washed with ethanol. The isolated samples were characterized by PXRD and IR spectroscopy.

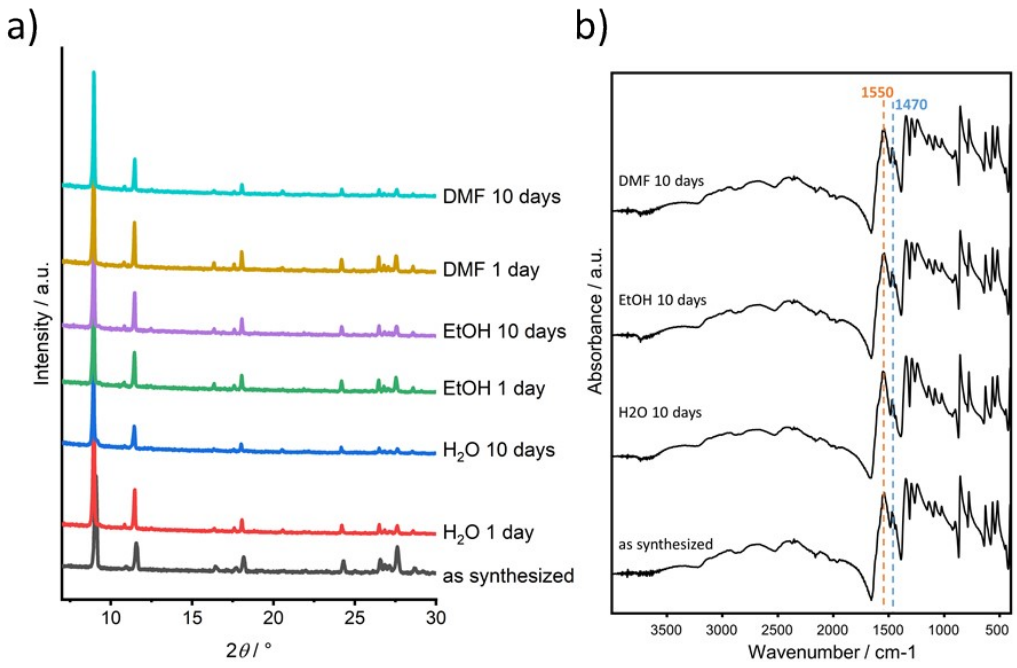

Figure S15. PXRD patterns (a) and FTIR spectra (b) after stability tests for (DMA){Fe(DSBDC)}.

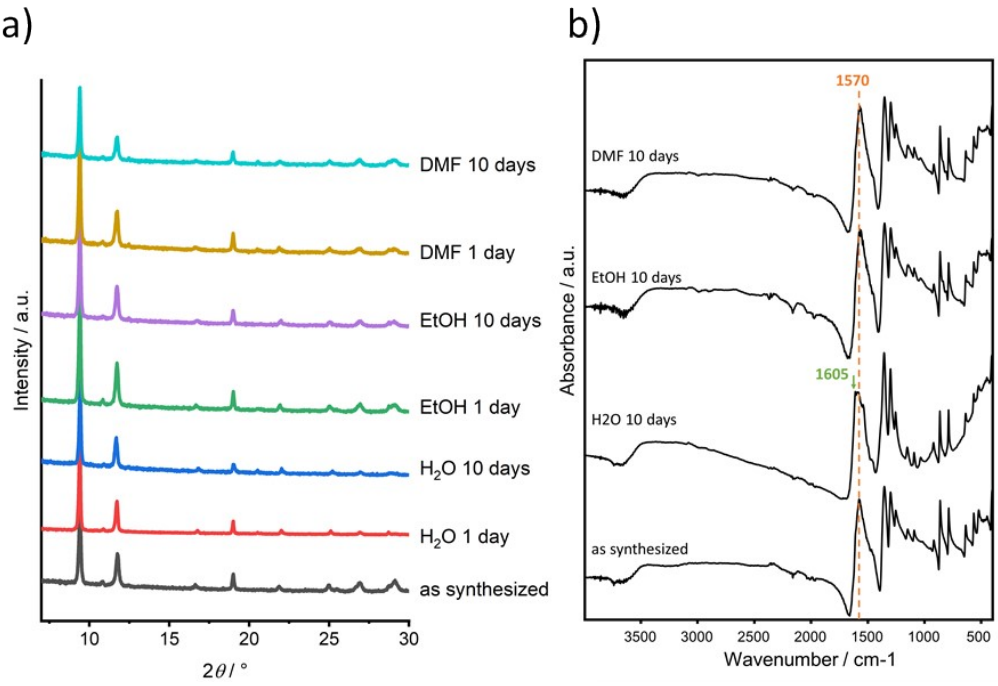

Figure S16. PXRD patterns (a) and FTIR spectra (b) after stability tests for Na{Fe(DSBDC)}·2.5H_2O.

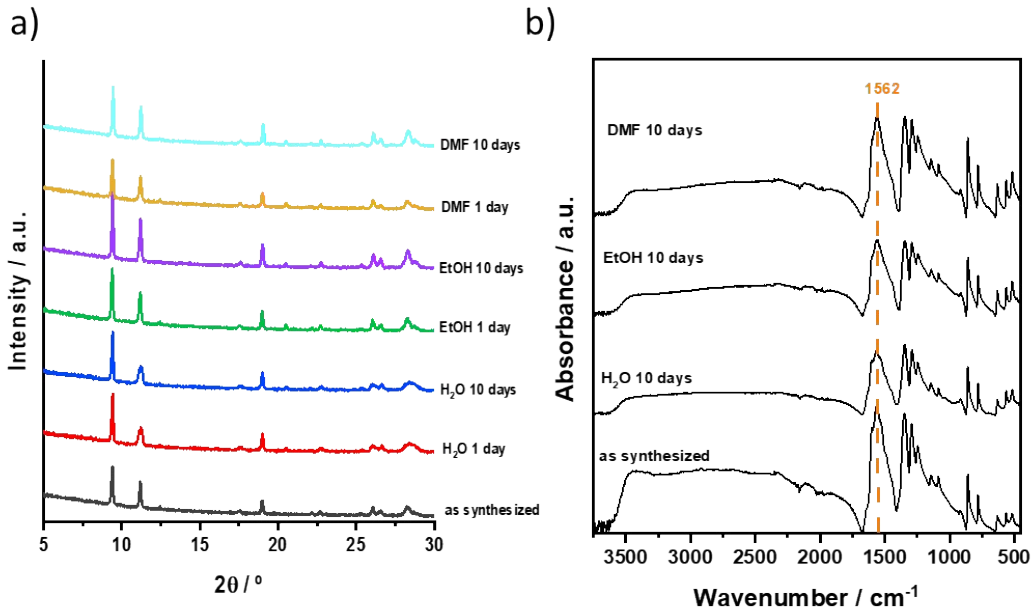

Figure S17. PXRD patterns (a) and FTIR spectra (b) after stability tests for K{Fe(DSBDC)}·nH_2O.

9. UV-vis absorption spectroscopy

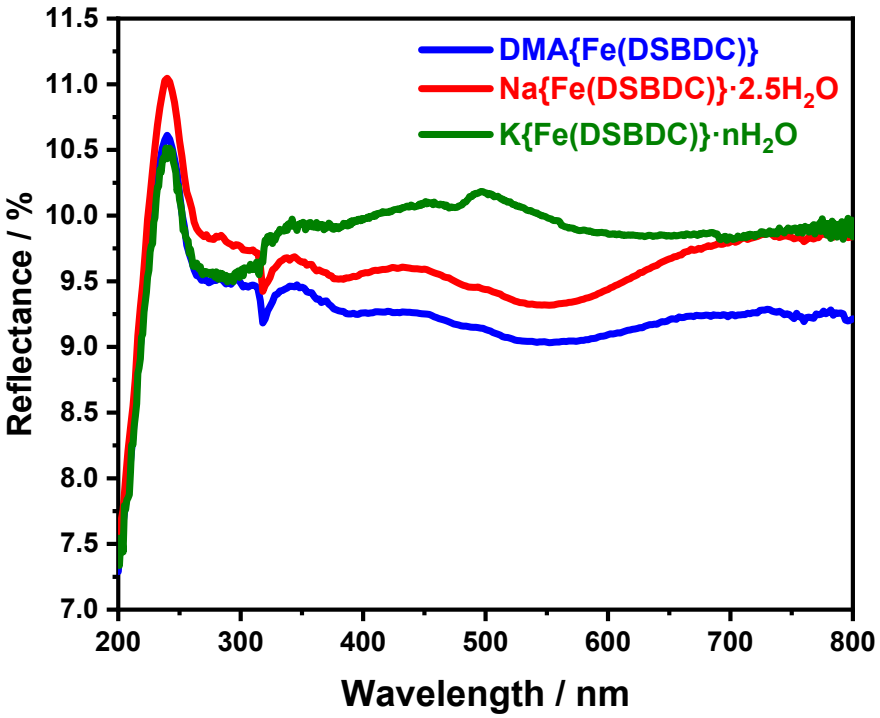

Figure S18. Solid-state UV-visible reflectance spectra of (DMA){Fe(DSBDC)}, Na{Fe(DSBDC)}·2.5H_2O and K{Fe(DSBDC)}·nH_2O.

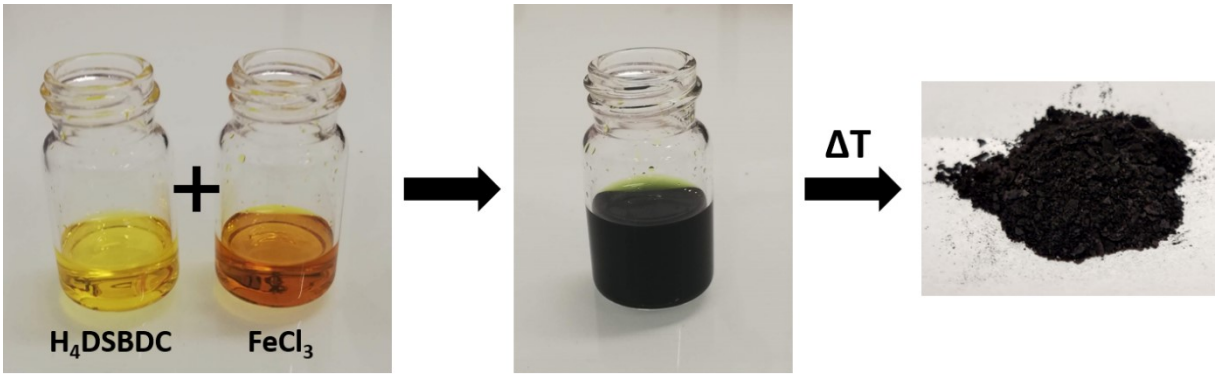

Figure S19. Illustration of the colour change occurring upon reaction between H_4DSBDC and Fe(III). Left: initial solution of reactants (in DMF): middle: solution after immediate mixing; right: powder recovered after heating (here Na{Fe(DSBDC)}·2.5H_2O.

10. Magnetic susceptibility and Mössbauer spectroscopy

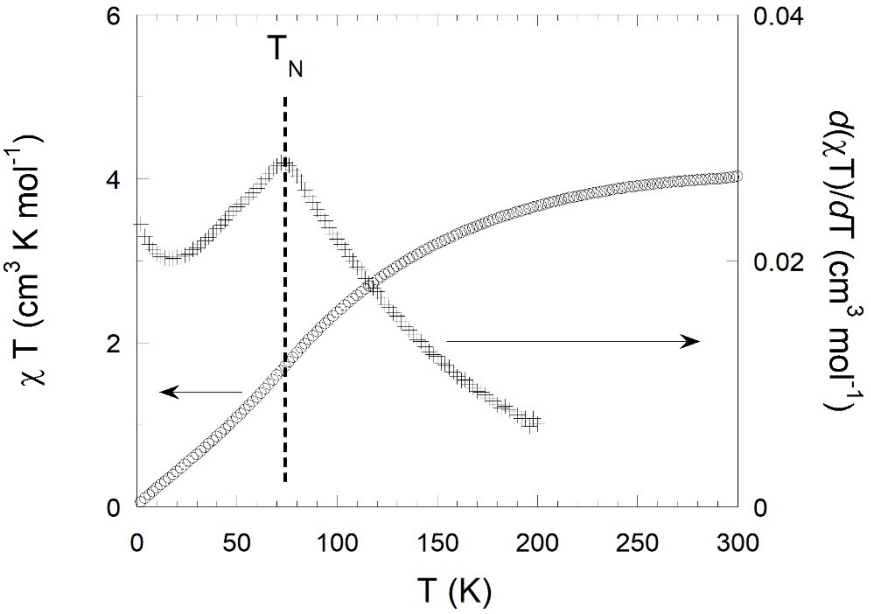

Figure S20. $\chi(T).T$ product for a Na{Fe(DSBDC)}·2.5H_2O sample as a function of temperature T (open circles; left scale). The derivative d($\chi(T).T$)/dT (plus signs; right scale) is also plotted to highlight the magnetic transition at $T_N \approx 72$ K.

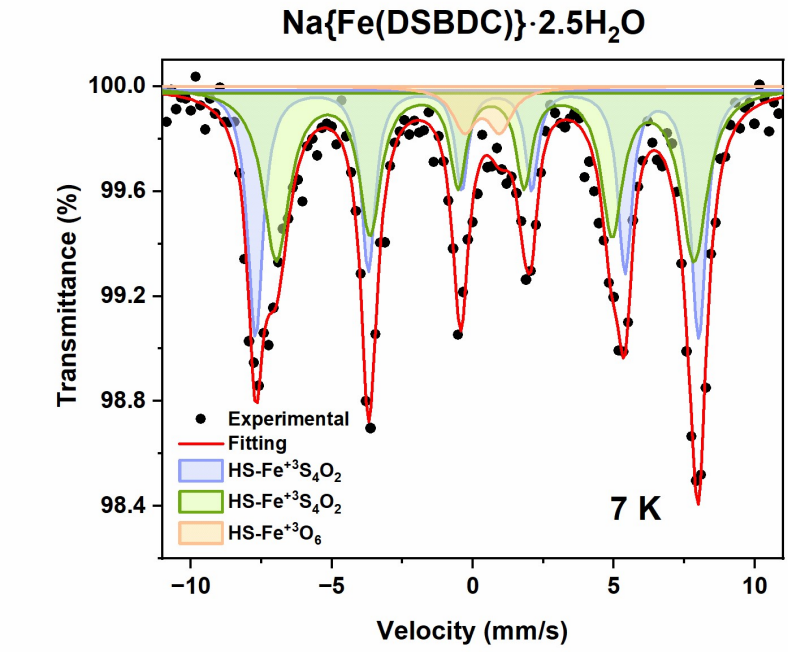

Figure S21. Mössbauer spectra of Na{Fe(DSBDC)}·2.5H_2O recorded at 7K.

Table S6. Refined values of hyperfine parameters of Na{Fe(DSBDC)}·2.5H_2O at 7K. At low temperature, magnetic ordering runs along the edge-sharing $\{FeS_4O_2\}_n$ chains and FeS_4O_2 sites are split into two inequivalent positions. On the other hand, FeO_6 sites are not affected by this magnetic ordering as they are not in direct contact with $\{FeS_4O_2\}_n$ chains.

	Hyperfine field B_{hf} (T)	**Δ (mm·s^{-1})**	**δ (mm·s^{-1})**	**Area (%)**	**Assignment**
Sextet # 1 (Blue)	48.76	-0.70	0.61	43	HS-$Fe^{+3}S_4O_2$
Sextet #2 (Green)	45.96	-0.21	0.65	51	HS-$Fe^{+3}S_4O_2$
Doublet		1.27	0.44	6	HS-$Fe^{+3}O_6$

11. Electrochemical evaluation

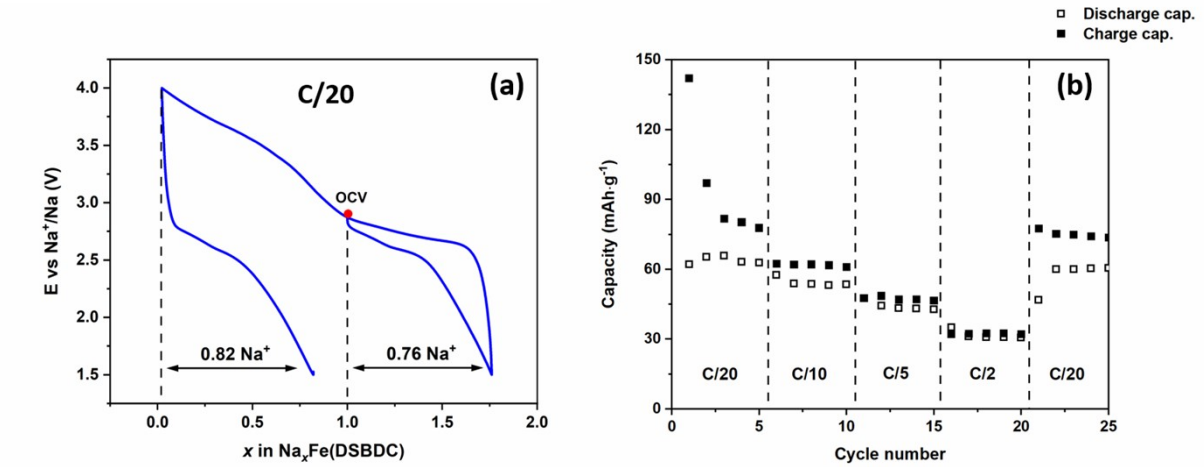

Figure S22. Electrochemical behavior of Na{Fe(DSBDC)} in a half-cell vs. Na cycled in a voltage range of 1.5–4.0 V vs. Na^+/Na. a) Potential vs. number of inserted/extracted Na^+ in the first cycle at C/20 current rate. b) Charge/discharge capacity at different current rates.

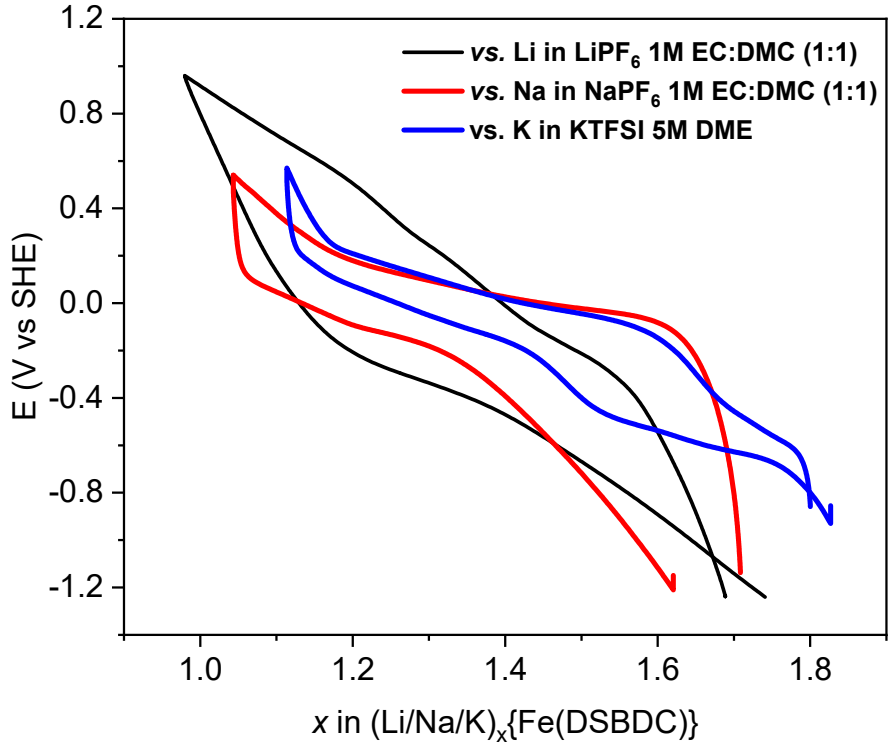

Figure S23. Comparison of the potential vs. number of inserted/extracted alkali cations during the first electrochemical cycle for the three alkali. The voltage axis refers to standard hydrogen electrode (SHE) .

References

(1) Vial, L.; Ludlow, R. F.; Leclaire, J.; Pérez-Fernandez, R.; Otto, S. Controlling the Biological Effects of Spermine Using a Synthetic Receptor. *J. Am. Chem. Soc.* **2006**, *128* (31), 10253–10257. https://doi.org/10.1021/ja062536b.

(2) Du, S.; Cui, M.; He, Z. Approach toward Iron(II) Coordination Polymers Based on Chain Motifs with Thiolate or Mixed Thiolate/Carboxylate Bridges: Structures and Magnetic Properties. *Inorg. Chem.* **2021**, *60* (24), 19053–19061. https://doi.org/10.1021/acs.inorgchem.1c02905.

(3) Sun, L.; Hendon, C. H.; Minier, M. A.; Walsh, A.; Dincă, M. Million-Fold Electrical Conductivity Enhancement in Fe 2 (DEBDC) versus Mn 2 (DEBDC) (E = S, O). *J. Am. Chem. Soc.* **2015**, *137* (19), 6164–6167. https://doi.org/10.1021/jacs.5b02897.

(4) Férey, G.; Millange, F.; Morcrette, M.; Serre, C.; Doublet, M.-L.; Grenèche, J.-M.; Tarascon, J.-M. Mixed-Valence Li/Fe-Based Metal–Organic Frameworks with Both Reversible Redox and Sorption Properties. *Angew. Chemie Int. Ed.* **2007**, *46* (18), 3259–3263. https://doi.org/10.1002/anie.200605163.

(5) Fateeva, A.; Horcajada, P.; Devic, T.; Serre, C.; Marrot, J.; Grenèche, J. M.; Morcrette, M.; Tarascon, J. M.; Maurin, G.; Férey, G. Synthesis, Structure, Characterization, and Redox Properties of the Porous MIL-68(Fe) Solid. *Eur. J. Inorg. Chem.* **2010**, *68* (24), 3789–3794. https://doi.org/10.1002/ejic.201000486.

(6) Yamada, T.; Shiraishi, K.; Kitagawa, H.; Kimizuka, N. Applicability of MIL-101(Fe) as a

Cathode of Lithium Ion Batteries. *Chem. Commun.* **2017**, *53* (58), 8215–8218. https://doi.org/10.1039/C7CC01712J.

(7) Sava Gallis, D. F.; Pratt III, H. D.; Anderson, T. M.; Chapman, K. W. Electrochemical Activity of Fe-MIL-100 as a Positive Electrode for Na-Ion Batteries. *J. Mater. Chem. A* **2016**, *4* (36), 13764–13770. https://doi.org/10.1039/C6TA03943J.